Applied Physics Express

LETTERS • **OPEN ACCESS**

Few-mode vertical-cavity surface-emitting laser: Optional emission of transverse modes with different polarizations

OPEN ACCESS

Applied Physics Express **11**, 052702 (2018)

https://doi.org/**10.7567/APEX.11.052702**

Few-mode vertical-cavity surface-emitting laser: Optional emission of transverse modes with different polarizations

Chuyu Zhong[1,2], Xing Zhang[1*], Werner Hofmann[3], Lijuan Yu[4], Jianguo Liu[4*], Yongqiang Ning[1], and Lijun Wang[1]

[1]*State Key Laboratory of Luminescence and Applications, Changchun Institute of Optics, Fine Mechanics and Physics, Changchun 130033, China*
[2]*University of Chinese Academy of Sciences, Beijing 100049, China*
[3]*Institut für Festkörperphysik und Zentrum für Nanophotonik, Technical University of Berlin, 10623 Berlin, Germany*
[4]*State Key Laboratory of Integrated Optoelectronics, Institute of Semiconductors, Beijing 100083, China*

*E-mail: zhangx@ciomp.ac.cn; jgliu@semi.ac.cn

Received March 12, 2018; accepted March 29, 2018; published online April 13, 2018

Few-mode vertical-cavity surface-emitting lasers that can be controlled to emit certain modes and polarization states simply by changing the biased contacts are proposed and fabricated. By directly etching trenches in the p-doped distributed Bragg reflector, the upper mesa is separated into several submesas above the oxide layer. Individual contacts are then deposited. Each contact is used to control certain transverse modes with different polarization directions emitted from the corresponding submesa. These new devices can be seen as a prototype of compact laser sources in mode division multiplexing communications systems. © 2018 The Japan Society of Applied Physics

The vertical-cavity surface-emitting laser (VCSEL), a key component for a variety of applications,[1–4] can intrinsically support multiple transverse modes through its large transverse dimension, which is usually an undesirable property in most applications. However, for some applications where laser sources are employed in the form of an array,[5] such as optical fiber communications using multiplexing technologies, including mode division multiplexing (MDM),[6–8] this unwanted feature could instead be beneficial.

MDM technology, in which information is selectively loaded on different spatial modes and transferred in a single-core few-mode fiber (FMF),[9] is expected to solve the problem that the capacity of commercial single-mode-fiber-based optical networks is reaching its limit. Like other multiplexing technologies, MDM requires multiplexers (MUXs) to convert multiple signals from a VCSEL array into a single fiber. Therefore, to ensure applicability to MDM communication systems, it is meaningful and feasible to develop a new type of VCSEL with multiple individually controllable modes, which can remove the need for a VCSEL array and greatly simplify or even eliminate the need for MUXs. Further, the polarization dynamics of the VCSEL are closely associated with the transverse modes,[10–12] so this type of VCSEL could also provide orthogonal fiber modes for MDM.

Various types of densely packed VCSEL arrays for high-speed communication have been fabricated. These arrays must have a small footprint for efficient fiber coupling. However, some of them[13,14] are not compact enough to be coupled into FMFs without sophisticated coupling optics. Ultrahigh-density VCSEL arrays with pie-shaped elements[15,16] have been fabricated, but in the design, only up to three mesas can be fitted into one fiber core. Photonic crystal and proton-implanted coherently coupled VCSEL arrays[17] with satisfactory properties have been reported. However, the need for complex fabrication limits the yield and potentially results in a high fabrication cost. Similar-looking devices with deeply etched petals have been presented,[18] but these devices focus on high-power single-mode output and are not suitable for MDM.

In this work, we present VCSELs with several emission-controllable transverse modes obtained by directly etching a few air gaps from the top. The upper mesa is separated into several submesas acting as waveguides, each of which is deposited with p-type contacts. Two types of few-mode VCSEL with three and four submesas are fabricated. Single-mode emission control of each submesa is achieved under certain driving current scales. Furthermore, polarization-controllable emission is achieved owing to the transverse-mode-related polarization of a VCSEL. The few-mode VCSELs with several pie-shaped submesas in a circle can naturally emit different transverse modes together with different polarization directions.

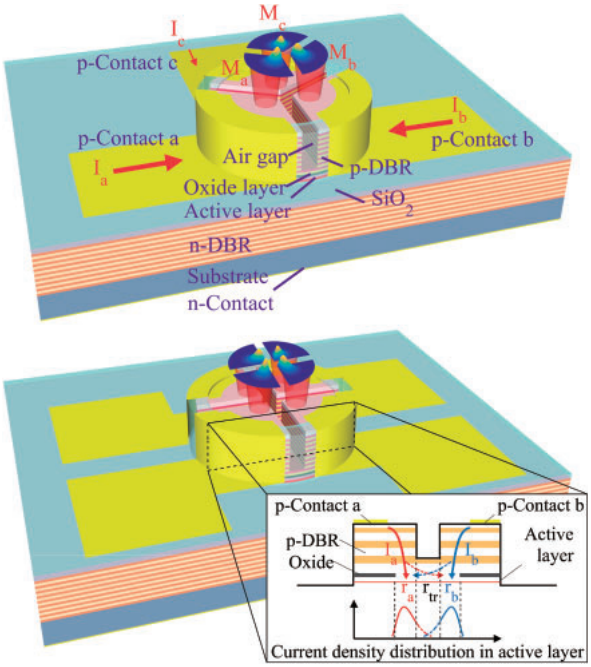

Fig. 1. Three-dimensional sketch of three-mode and four-mode VCSELs. When a current I_a is injected through p-contact a, mode a (M_a) is emitted, and so forth for p-contacts b and c. Lasing region a (r_a) corresponds to M_a and so on for other lasing regions and modes. The inset shows the current flow inside the device, where r_{tr} is the region directly under the trench.

The three-dimensional structures of our few-mode VCSELs are schematically illustrated in Fig. 1. For example, in the three-mode VCSEL, the upper mesa is divided into three

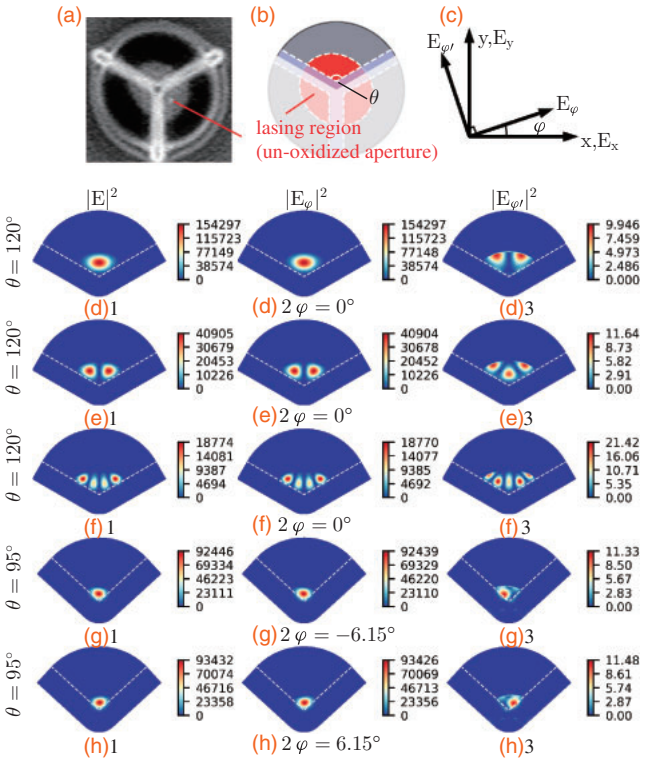

Fig. 2. Mode analysis of various type of single lasing regions. (a) Infrared microscope image of the mesa after steam oxidation. Black areas are the oxide layer, and the three gray regions belong to the un-oxidized aperture. (b) Simulation geometry. The red pie-shaped area is the lasing region, the gray area is the Al_xO, and the light purple region represents the high-loss area under the trench. θ is the opening angle between trenches. (c) Annotation of the polarization directions of different electric field components. (d1)–(h1) Mode patterns of the total electric field E. Intensity distribution of (d2)–(h2) the major polarization component E_φ and (d3)–(h3) the minor polarization component $E_{\varphi'}$. Lasing regions in (d), (e), and (f) are symmetric, whereas those in (g) and (h) are nonsymmetric. $\varphi' = \varphi + 90°$. The white dashed lines in (d)–(h) indicate the interface between the submesa and air gap.

lobes (submesas) by air trenches, and p-contacts are deposited above them. As mentioned in our previous work on the two-mode VCSEL,[19] the air gaps provide extra current isolation and carrier-distribution guidance. Therefore, the trenches enable an inhomogeneous carrier distribution in the active region, where the laser can emit only if the carrier density is sufficient, because the optical modes in an oxide-confined VCSEL are governed in part by the relationship between the optical field and carrier distribution.[20] In addition, the air trench affords optical restriction. From the air gap (r_{tr}), only fluorescence is emitted because of the low reflectivity. Laser light is stimulated from lasing regions r_a, r_b, and r_c when current is injected from the corresponding contact. These regions are located in the active layer, and their sizes and shapes are determined directly by the sizes and directions of the air trenches together with the oxide aperture. Because of the anisotropy of the oxidation speed of the oxide layer, the oxide aperture has an elliptical shape. Therefore, the pie-shaped lasing regions can be nonsymmetrical, as shown in Fig. 2(a).

To understand how the geometry of the lasing region affects the transverse mode, mode analysis of submesas with lasing regions of different sizes and shapes was performed using COMSOL Multiphysics®. The first three eigenmodes

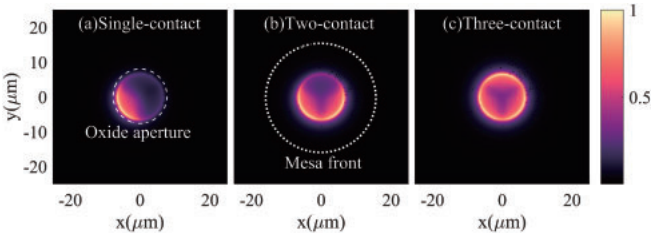

Fig. 3. Calculated normalized current density distribution in active layer under (a) single-contact, (b) two-contact, and (c) three-contact injection.

of the submesa with a 120°-opening-angle lasing region are depicted in Figs. 2(d)–2(f). Owing to the region's symmetry, they are all x-polarized. In the 95° one shown in Figs. 2(f) and 2(h), the polarization directions of the fundamental modes are $\mp 6.15°$ off of the x-axis because the shape is set to be nonsymmetric. In fact, each eigenmode of a certain lasing region in Fig. 2 has two solutions, both of which have almost the same intensity distribution but orthogonal polarizations, and we show only one of them. However, we can still refer to the simulation results to achieve manipulation of both the transverse modes and polarization of a single VCSEL device by properly controlling the size of the oxide aperture and the direction of the trenches.

The current flow inside our device was also simulated, and the normalized current density distributions on the active layer under different injection conditions are shown in Fig. 3; they indicate that current crosstalk between submesas is small. The carrier density of the active regions under the unbiased submesas should be far from sufficient to excite the laser, guaranteeing independent emission control of each p-contact.

The main fabrication process of the few-mode devices is the same as that of a normal VCSEL, except for an additional step of air gap etching by inductively coupled plasma. To control the shapes and sizes of the trenches more precisely, trench etching was performed in the first step. The depth of the trench is approximately 2.3 μm, whereas the oxide layer and active layer are 2.65 and 2.79 μm deep, respectively. Because the trench bottom is so close to the oxide layer, the width of the air gaps can be designed to be as narrow as 2 and 3 μm, whereas they got about 0.2 μm widened.

All measurements were performed under continuous-wave (CW) operation at room temperature. I_i (i = a, b, c, or d) indicates that only contact-i is biased. I_{ij} (i,j = a, b, c, or d, $i \neq j$) indicates that both contact-i and contact-j are biased, and so forth for I_{ijk} and I_{ijkl}. The measured near fields of the three-mode VCSEL are depicted in Fig. 4. The irregular profiles of the lasing regions and fluorescence from the trenches can be seen below threshold in Fig. 4(a). Although fluorescence from the trenches exists under all the types of injection, it is nearly invisible above threshold because neutral density filters with various extinction ratios were used to avoid saturation of the CCD camera by the laser. The near fields under I_a, I_b, and I_c injection are displayed in Figs. 4(b), 4(c), and 4(d), respectively. I_i injection successfully produced only mode M_i emission coinciding with the near fields under multicontact injection, which are shown in Figs. 4(e)–4(h). In summary, the three-mode VCSEL has seven types of operation: three types of single-mode operation, three types of two-mode operation, and one type of three-mode operation.

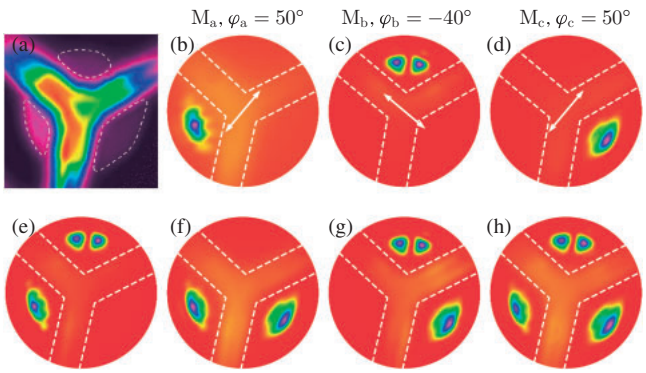

Fig. 4. Near fields of a three-mode VCSEL. (a) Near-field pattern below threshold, where lasing regions can be observed and are enclosed in dashed lines. (b)–(d) Near fields under I_a, I_b, and I_c injection, respectively. The arrows show the polarization directions of M_φ. (e)–(h) Near-field profiles under I_{ab}, I_{ac}, I_{bc}, and I_{abc} injection, respectively.

Table I. Major polarization angle under different types of injection.

	I_a	I_b	I_c
I_a	50°	M_a: 50°, M_b: 50° or −40°	M_a: −40°, M_c: 50°
I_b	—	−40°	M_a, M_c: 50°
I_c	—	—	50°

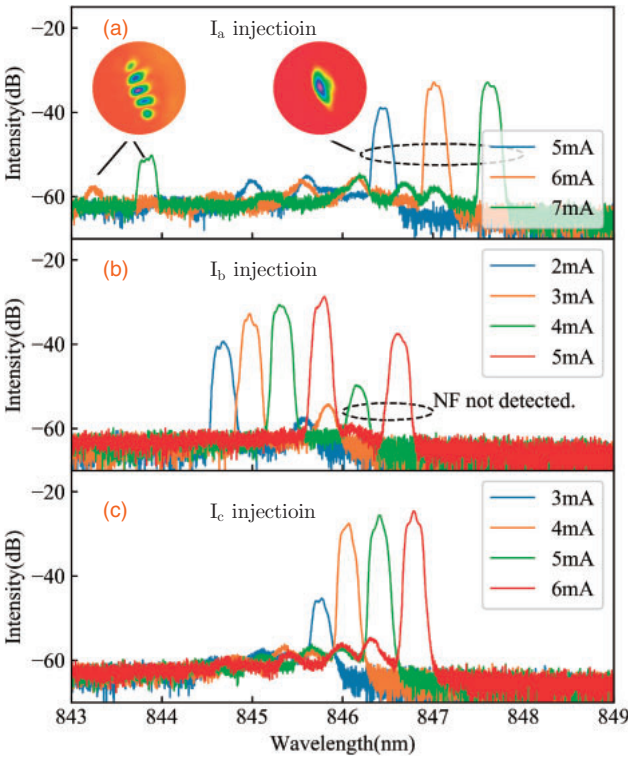

Fig. 5. Spectra of three-mode VCSEL under single-contact injection. (a) Spectra under I_a injection from 5 to 7 mA. Insets show the fundamental mode and a high-order mode. (b) Spectra under I_b injection from 2 to 5 mA. (c) Spectra under I_c injection from 3 to 6 mA.

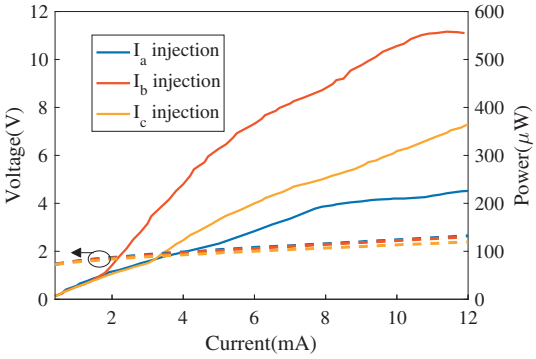

Fig. 6. CW *L–I–V* performance of three-mode VCSEL.

The polarization directions at each injection condition are summarized in Table I. Under single-contact injection, the main polarization directions of M_a, M_b, and M_c are 50, −40, and 50°, respectively. Because of the nonsymmetrical geometry, the polarization directions are neither along nor orthogonal to the angle bisector of the tip of r_a and r_b. The minor component of M_a is relatively obvious, but its magnitude is still small compared to the major component, as shown in Fig. 5(a). Interestingly, it is the second-order mode [see Figs. 2(c) and 4(c)] rather than the fundamental mode that is the first excited mode of r_b. As shown in Fig. 5(b), there are two peaks in the spectra of M_b under 5 mA, but we can observe only the near field of the second-order mode, which is the major polarization component under full current scale. Further, only I_c injection can achieve single-mode emission at full current scale, which is evident in Fig. 5(c). Therefore, every contact can be controlled to achieve single-mode, single-polarization emission at certain driving currents. Under multicontact injection, the polarizations of some transverse modes shifted. I_{ab} injection was unstable, as the major polarization of M_b switched between 50 and −40° from time to time, whereas M_a had stable polarization at 50°. Under I_{ac} injection, M_a switched to stable polarization at −40°, and M_c remained polarized at 50°. Under I_{bc} injection, both M_b and M_c were polarized at 50°. I_{ac} injection resulted in emission with two controllable orthogonal polarizations.

The CW *L–I–V* characteristics of the three-mode VCSEL are shown in Fig. 6. When laser modes propagate from the active layer to the output window, they suffer from scattering loss from the air trenches. Modes excited from lasing regions with a larger aspect ratio have a higher field intensity at the edges, resulting in more loss. However, the larger size can help complement the power. This behavior explains the differences among the power curves of r_a, r_b, and r_c.

In agreement with our expectation, mode control of a four-mode VCSEL was also achieved, as shown in Fig. 7. By investigating the spectra under single-contact injection, we demonstrated single-mode emission from three submesas. Submesas a and b can maintain single-mode operation at full current scale, as shown in Figs. 7(a) and 7(b). From Fig. 7(c), we see that single-mode operation remained until the driving current reached 4.5 mA for submesa c. The largest region, submesa d, exhibited two-mode emission at full scale, as illustrated in Figs. 7(d) and 7(h), implying that the direction of the air gaps can be modified. The peak of $M_{\varphi'}$ for M_d is higher than the M_φ values in the spectrum owing to differences in the coupling efficiency of different transverse modes; that is, the fundamental mode has better coupling than higher-order modes. The near fields and the corresponding polarizations are displayed in Figs. 7(e)–7(h). Independent control of three polarizations in a single device was realized, and two of the polarization directions are orthogonal. Although it is not demonstrated, the four-mode VCSEL can operate under 15 injection conditions, that is, in 15

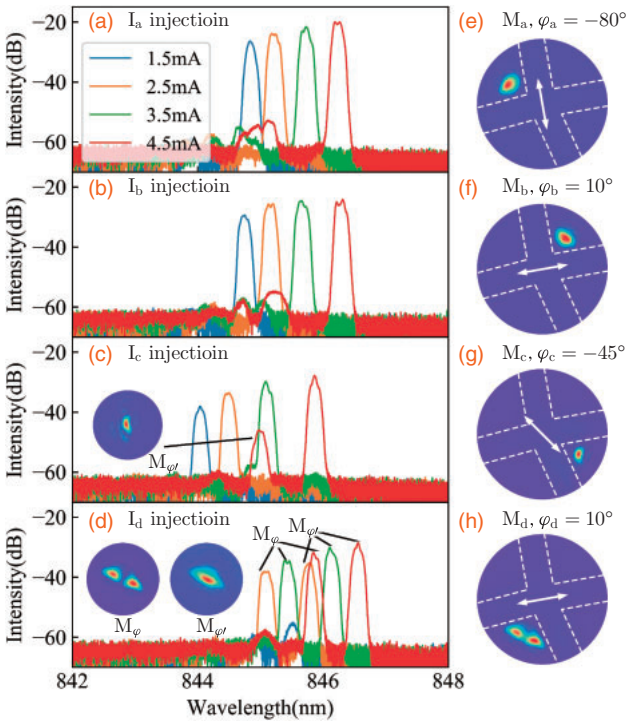

Fig. 7. Spectra and near-field profiles of four-mode VCSEL for different single-contact injection conditions. (a)–(d) Spectra for each type of single-contact injection from 1.5 to 4.5 mA. (e)–(h) Near fields under I_a–I_d injection. Inset in (c) shows the minor component of M_c under 4.5 mA, and insets in (d) show the major and minor components of M_d.

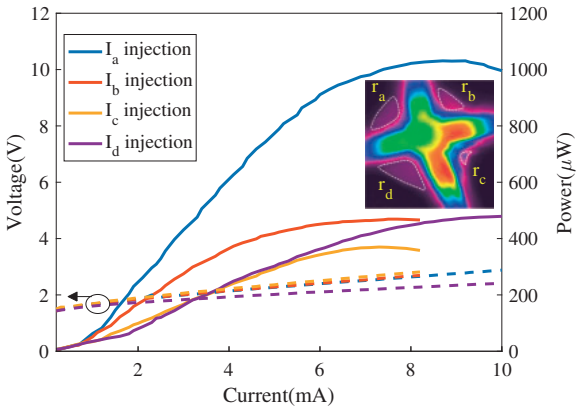

Fig. 8. CW *L–I–V* performance of four-mode VCSEL. Inset shows the near-field profile below threshold.

transverse mode combinations. Finally, the *L–I–V* curves are shown in Fig. 8, from which we can also differentiate the lasing regions by their geometries. Improved single-mode power compared to the three-mode device was achieved.

In summary, VCSELs with several independent contacts that can control the emission of certain transverse modes and different polarizations independently were demonstrated. The shape and direction of each lasing region were proven to have a decisive impact on the transverse mode formation and polarization direction. The functionality of current guidance and optical field restriction of the air gap enable the independent emission control. Near-field profiles and spectra under single-contact injection and multicontact injection indicated that the emission status of the few-mode VCSEL can be manipulated by simply shifting the biased contact, and the VCSEL can be switched from single-mode operation to few-mode operation. We believe that our few-mode VCSEL prototype will contribute to future optical communication systems.

Acknowledgments This work is supported by the National Basic Research Program of China (No. 2014CB3400102), the National Natural Science Foundation of China (NSFC) (Nos. 61434005, 61474118, 11774343, and 11674314), the Youth Innovation Promotion Association, CAS (No. 2017260), and the Chinese Academy of Sciences President's International Fellowship Initiative (No. 2018VTA0005).

1) D. K. Serkland, K. M. Geib, G. M. Peake, R. Lutwak, A. Rashed, M. Varghese, G. Tepolt, and M. Prouty, Proc. SPIE **6484**, 648406 (2007).
2) D. K. Serkland, G. M. Peake, K. M. Geib, R. Lutwak, R. M. Garvey, M. Varghese, and M. Mescher, Proc. SPIE **6132**, 613208 (2006).
3) H. H. Lu, C. Y. Li, C. A. Chu, T. C. Lu, B. R. Chen, C. J. Wu, and D. H. Lin, Opt. Lett. **40**, 4563 (2015).
4) J.-F. Seurin, G. Y. Xu, Q. Wang, B. M. Guo, R. Van Leeuwen, A. Miglo, P. Pradhan, J. D. Wynn, V. Khalfin, and C. Ghosh, Proc. SPIE **7615**, 76150F (2010).
5) A. Larsson, P. Westbergh, J. S. Gustavsson, E. Haglund, and E. P. Haglund, Proc. SPIE **9381**, 93810D (2015).
6) K. Szczerba, P. Westbergh, M. Karlsson, P. A. Andrekson, and A. Larsson, J. Lightwave Technol. **33**, 1395 (2015).
7) D. M. Kuchta, A. V. Rylyakov, F. E. Doany, C. L. Schow, J. E. Proesel, C. W. Baks, P. Westbergh, J. S. Gustavsson, and A. Larsson, IEEE Photonics Technol. Lett. **27**, 577 (2015).
8) B. Zhu, T. F. Taunay, M. F. Yan, M. Fishteyn, G. Oulundsen, and D. Vaidya, IEEE Photonics Technol. Lett. **22**, 1647 (2010).
9) H. Chen and A. M. J. Koonen, *Fibre Optic Communication: Key Devices* (Springer, Cham, 2017) p. 1.
10) H. Li, T. L. Lucas, J. G. McInerney, and R. A. Morgan, Chaos Solitons Fractals **4**, 1619 (1994).
11) M. San Miguel, Q. Feng, and J. V. Moloney, Phys. Rev. A **52**, 1728 (1995).
12) J. Martín-Regalado, S. Balle, M. San Miguel, A. Valle, and L. Pesquera, Quantum Semiclass. Opt. **9**, 713 (1997).
13) S. Y. Hu, J. Ko, E. R. Hegblom, and L. A. Coldren, IEEE J. Quantum Electron. **34**, 1403 (1998).
14) Y. G. Ju, D. Lofgreen, A. Fiore, S. Y. Hu, E. Hegblom, D. Louderback, O. Sjolund, A. Huntington, and L. A. Coldren, IEEE Photonics Technol. Lett. **12**, 462 (2000).
15) H. Roscher, P. Gerlach, F. N. Khan, A. Kroner, M. Stach, A. Weigl, and R. Michalzik, Proc. SPIE **6185**, 61850V (2006).
16) H. Roscher, F. Rinaldi, and R. Michalzik, IEEE J. Sel. Top. Quantum Electron. **13**, 1279 (2007).
17) M. T. Johnson, D. F. Siriani, M. P. Tan, and K. D. Choquette, Appl. Phys. Lett. **103**, 201115 (2013).
18) A. Furukawa, S. Sasaki, M. Hoshi, A. Matsuzono, K. Moritoh, and T. Baba, Appl. Phys. Lett. **85**, 5161 (2004).
19) C. Zhong, X. Zhang, L. Yu, J. G. Liu, W. Hofmann, Y. Ning, and L. Wang, IEEE Photonics Technol. Lett. **29**, 1840 (2017).
20) C. Degen, W. Elsaber, and I. Fischer, Opt. Express **5**, 38 (1999).